Optical Materials 108 (2020) 110213

Contents lists available at ScienceDirect

Optical Materials

journal homepage: http://www.elsevier.com/locate/optmat

An optimized lead-free formamidinium Sn-based perovskite solar cell design for high power conversion efficiency by SCAPS simulation

Manish Kumar [a,*], Abhishek Raj [b,c], Arvind Kumar [a], Avneesh Anshul [b,**]

[a] Experimental Research Laboratory, Department of Physics, ARSD College, University of Delhi, New Delhi, 110021, India
[b] CSIR-National Environmental Engineering Research Institute (NEERI), Nagpur, 440020, India
[c] Academy of Scientific and Innovative Research (AcSIR), Ghaziabad, 201002, India

ARTICLE INFO

Keywords:
SCAPS simulation
Lead-free perovskite solar cell
Power conversion efficiency
I–V characteristics
Electron transport layer
Hole transport layer

ABSTRACT

An organic-inorganic perovskite formamidinium tin iodide ($HC(NH_2)_2SnI_3$– $FASnI_3$) is used as light absorbing layer in photovoltaics due to its lead-free nature, wider bandgap of 1.41 eV and better temperature stability than $CH_3NH_3SnI_3$. In the present investigations, SCAPS simulation with comparison to the experimental as well as simulation data for $FASnI_3$-based solar cell device is accomplished for high power conversion efficiency with proper optimization. The variation in the device design key parameters such as absorber, hole transport layer and electron transport layer thickness including defect density, doping concentration in absorber, carriers capture cross sections and interfacial defects are examined with their impact on device performance. The preliminary structure of device is based on the reported experimental and simulation work with the efficiency of 1.75% and 1.66%, respectively. After the SCAPS simulation with the optimization of basic parameters in this work, the final optimized performance parameters of the solar cell device are found to be enhanced with short-circuit current density (J_{sc}) of 31.20 mA/cm^2, open-circuit voltage (V_{oc}) of 1.81 V, fill factor (%FF) of 33.72% and power conversion efficiency (%PCE) of 19.08%.

1. Introduction

In recent years, methylammonium lead halide perovskite solar cells have received remarkable attention over worldwide due to their exceptional properties such as high extinction coefficient, solution processable fabrication techniques, appropriate band gap and tremendous enhancement in power conversion efficiency (PCE) [1–3]. To date, the PCE of perovskite based solar cell devices reached to 25.2% which was initially just 3.8% in 2009 [4,5]. This significant achievement brought perovskite solar cell as a strong competitor of Si-based solar cell in photovoltaic market [6,7].

However, presence of toxic heavy metal like lead associated over whole lifecycle of perovskite solar cells (PSCs) is the major concern from environment perspective [8]. Therefore, considerable effort is being required to introduce non-toxic element in perovskite photovoltaic [9]. Fortunately, various type of less toxic cations such as Sn(II), Bi(III), Ti (IV), Sb(III) and Ge(II) have demonstrated as a substitute of lead in PSCs. Recent implementation of cesium tin iodide ($CsSnI_3$), formamidinium tin iodide ($FASnI_3$) and methylammonium tin iodide ($MASnI_3$) with direct band gap of approximate 1.3eV, 1.41eV, and 1.20eV in PSC have open up the way towards non-toxic PSCs. Amongst these photovoltaic contenders, Sn-based halide perovskite has got more consideration due to their similar property like lead halide PSCs and excellent PCE. But degradation of Sn-based devices is another obstacle in this field when exposure in ambient atmosphere [10–12].

Neol et al. [13] have reported fully lead-free $CH_3NH_3SnI_3$ based PSC and exhibited PCE of 6%. The device was fabricated in closed nitrogen filled glove box to avoid the possibility of exposure to air, through spin coating process with cell configuration of FTO/c-TiO_2/mp--TiO_2/$CH_3NH_3SnI_3$/Spiro-OMeTAD/Au. It has observed that under ambient atmospheric environment, Sn^{2+} present in the light absorbing material rapidly and transformed into Sn^{4+} which is more stable state. As a result of this process, the charge neutrality of light absorbing material breaks which leads to the formation of SnO_2 and methylammonium iodide (MAI) [13]. Another study have reported the PCE of 5.73% with band gap engineered perovskite material of $CH_3NH_3SnI_{3-x}Br_x$ [14]. Similarly, Kumar et al. have reported PSC with $CsSnI_3$ active layer through vacancy modulation which is exhibited

* Corresponding author.
** Corresponding author.
E-mail addresses: manishphy2007@gmail.com, mkumar2@arsd.du.ac.in (M. Kumar), avneesh.anshul@gmail.com (A. Anshul).

https://doi.org/10.1016/j.optmat.2020.110213
Received 10 June 2020; Received in revised form 4 July 2020; Accepted 9 July 2020
Available online 6 August 2020

maximum power conversion efficiency of 2.02% but the complete processing and testing has been done in nitrogen filled glove box due to instability associated with $CsSnI_3$ [15]. To overcome the concern of temperature instability, Koh et al. have introduced formamidinium tin iodide ($HC(NH_2)_2$– SnI_3 – $FASnI_3$) based PSC with band gap of 1.41eV. The fabricated device exhibited PCE of 1.41% under optimized device structure with 20mol% of SnF_2 concentration. With the increase in thickness of electron transport layer TiO_2 up to 500 nm, an enhanced PCE of PSC reached to 2.10%. In the recent research, several approaches have been adopted to enhance the stability and PCE of the $FASnI_3$ based solar cell devices [16]. Ke et al. introduced diammonium cations in $FASnI_3$ based PSC, reported maximum PCE of 5.85% [17], Kayesh et al. have introduced hydrazinium chloride (N_2H_5Cl) in $FASnI_3$ active layer that diminished concentration of Sn^{4+} content by 20% [18].

Now a days, several theoretical studies have been performed to investigate the new pathway for Sn-based photovoltaic devices. Hima et al. have reported comparative study on $CH_3NH_3PbI_3$ and $CH_3NH_3SnI_3$ by using SILVACO ATLAS simulation software and exhibited PCE of 18.16% and 9.56%, respectively. The idea behind their study to optimize the thickness of light absorbing material to obtained the better result [19]. Abdelaziz et al. have studied the iodide ($HC(NH_2)_2$– SnI_3 – $FASnI_3$) based PSC through SCAPS simulation to investigate the impact of defect density, thickness and doping concentration on the performance of the device. The optimized device exhibited maximum PCE of 14.03% with open circuit voltage of 0.92 V, current density of 22.65 mA/cm^2 and fill-factor of 67.74% [20]. Despite of these studies, we have found that the device performance can be improve further by optimizing the PSCs parameters more precisely.

In the present simulation work, $FASnI_3$ based PSCs have been explored and analyzed the impact of thickness of absorber, hole transport layer (HTL) thickness, electron transport layer (ETL) thickness, defect density, doping concentration in absorber, carriers capture cross sections of carriers and interfacial defects on device performance. The major part of this study is to optimize the parameters of PSCs precisely in such a way that obtained device delivered enhanced PCE and reduced the fabrication cost.

2. Device structure and simulation methodology

2.1. Device structure

Present study is performed under AM1.5G illumination in SCAPS-1D (ver.3.3.07) simulation software, developed by University of Gent, Belgium. Although, simulation calculations carried out inside SCAPS-1D is mainly derived from three fundamental equations: Poisson equation, hole continuity equation and electron continuity equation. In SCAPS-1D, heterostructure solar cell can be design with seven different layers and simulation can be performed in both light and dark environmental conditions [21,22].

The device configuration of simulated solar cell FTO/TiO_2/$FASnI_3$ (Light absorbing layer)/Spiro-OMeTAD/Au, band diagram and grading of energy parameters are illustrated in Fig. 1 (a-c). In this device structure $FASnI_3$ acts like light harvesting material, inserted between HTL (Spiro-OMeTAD) and ETL (TiO_2). However, Fluorine-doped Tin Oxide (FTO) is used as front contact and gold (Au) thin layer as back metal contact.

2.2. SCAPS simulation methodology

Basic parameters used to perform simulation work are collected from various experimental and theoretical paper, summarized in Table 1 [16,19,20,23–36]. Fig. 2 depicts the initially optimized (with the theoretical and experimental data) [16,20], current-density vs voltage graph and the inset shows the corresponding quantum efficiency-wavelength graph. Some other parameters for $FASnI_3$ such that conduction band and valance band effective density of states (EDOS) are consider as 1 × 10^{18} cm^{-3} whereas electron and holes thermal velocities of all layers are taken as 10^{17} cm/s. Initial and total defect density of light absorbing layer are set as 2 × 10^{15} cm^{-3}. Interaction between two layers at interfacial point play a major role in the device performance. Table 2 listed the defect density of light absorbing layer and interferes as per the reported literature [19,20]. Table 3 represents the carriers (electrons and holes) capture cross section modified parameters across the ETL/perovskite layer interfaces. The PCE achieved for present simulation is 2.23% which is almost near to experimental PCE and previously reported theoretical PCE mention in Table 4. It has been observed from the simulation result that after modification in the carriers (electrons and holes) capture cross section of interfacial parameters at ETL/perovskite layer (modified present simulation), PCE of device has been reached to 5.27% from the 2.23%, included in Table 4. Keeping the thickness of HTL and ETL constant and varying the thickness of absorbing layer, the maximum PCE of 6.12% is achieved at 800 nm, listed in supplementary material (TS1). Supplementary material (TS2) includes the variation in

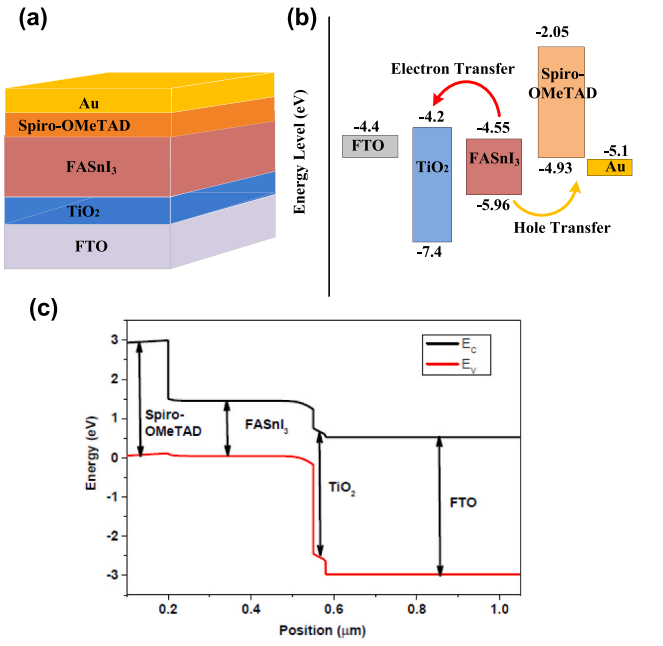

Fig. 1. (a) Device configuration of simulated PSC, (b) Energy band diagram of the device and (c) grading of energy parameters.

Table 1
Basic parameters of each layer of the device [16,19,20,24–36].

Material property	FTO	TiO_2	$FASnI_3$	Spiro-OMeTAD
Thickness 't' (nm)	500	30	350	200
Band gap 'E_g' (eV)	3.5	3.2	1.41	2.88
Electron affinity 'χ' (eV)	4	4	3.52	2.05
Dielectric Permittivity 'ε_r'	9	9	8.2	3
CB EDOS 'N_c' (cm^{-3})	2.2× 10^{18}	2.1 × 10^{18}	1.0× 10^{18}	2.2× 10^{18}
VB EDOS 'N_v' (cm^{-3})	1.8× 10^{19}	1.8× 10^{19}	1.0× 10^{18}	1.8× 10^{19}
Electron mobility 'μ_n' (cm^2/V.s)	20	20	22	2.0× 10^{-4}
Hole mobility 'μ_h' (cm^2/V.s)	10	10	22	2.0× 10^{-4}
Shallow donor density 'N_D' (cm^{-3})	2.0× 10^{19}	9.0× 10^{16}	0	0
Shallow Acceptor density 'N_A' (cm^{-3})	0	0	7.0× 10^{16}	2.0× 10^{19}
Defect density 'N_t' (cm^{-3})	1.0× 10^{15}	1.0× 10^{15}	2.0× 10^{15}	1.0× 10^{15}

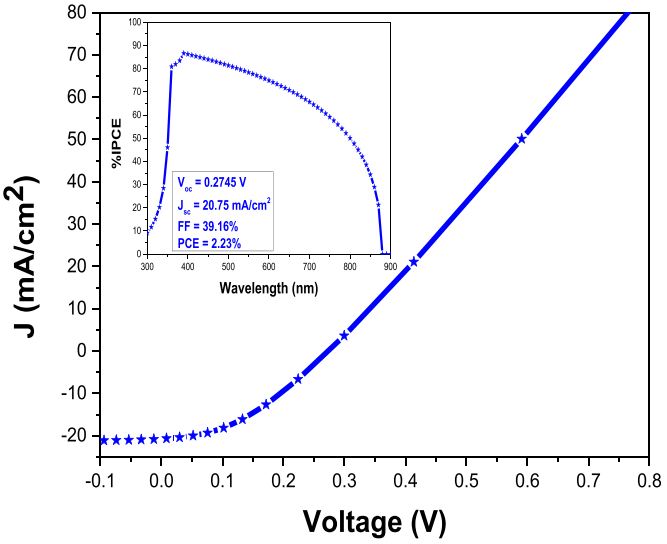

Fig. 2. Initially optimized current-density vs wavelength and quantum efficiency vs wavelength (inset) with experimental and theoretically reported results.

Table 2
Defect density values inside the absorber layer and at interface of the device [19,20].

Parameter	Absorber/ HTL	ETL/ Absorber	$FASnI_3$
Defect density	Neutral	Neutral	Neutral
Capture cross section for electron (cm^{-2})	1×10^{-15}	1×10^{-15}	2×10^{-14}
Capture cross section for hole (cm^{-2})	1×10^{-15}	1×10^{-15}	2×10^{-14}
Energetic distribution	Single	Single	Gaussian
Energy level with respect to E_v	0.60	0.60	0.65
Characteristic energy (eV)	NA	NA	0.1
Total density (cm^{-3})	1×10^{16}	1×10^{16}	2×10^{15}

Table 3
Modified defect density inside the absorber layer and at interface of the device.

Parameter	Absorber/ HTL	ETL/ Absorber	$FASnI_3$
Defect density	Neutral	Neutral	Neutral
Capture cross section for electron (cm^{-2})	1×10^{-15}	1×10^{-19}	2×10^{-14}
Capture cross section for hole (cm^{-2})	1×10^{-15}	1×10^{-19}	2×10^{-14}
Energetic distribution	Single	Single	Gaussian
Energy level with respect to E_v	0.60	0.60	0.65
Characteristic energy (eV)	NA	NA	0.1
Total density (cm^{-3})	1×10^{16}	1×10^{16}	2×10^{15}

Table 4
Performance parameters on the basis of basic parameters (present simulation) and defect density variation inside the absorber including at interface (modified present simulation) and also the comparison with latest experimental and theoretical literature.

Parameter	Experimental [16]	Simulation reports [20]	Present simulation	Modified present simulation
J_{sc} (mA/ cm^2)	15.85	14.45	20.75	21.42
V_{oc} (V)	0.264	0.261	0.2745	0.460
FF (%)	42	43.91	39.16	53.41
PCE (%)	1.75	1.66	2.23	5.27

ETL, HTL and absorber thickness to obtained enhanced PCE of the device. The variation in defect density with doping concentration also affects the device performance. In supplementary material (TS3), the defect density with doping concentration is varied from 1×10^{14} to 1×10^{16} cm^{-3} to obtained enhanced output of simulated PSC. Also, the efforts have been made to study that how variation in electron affinity of ETL and HTL affect the device operation which is shown in supplementary material (TS4). Finally, after optimizing the different parameter of simulated device, the maximum PCE of 19.08% is achieved and listed in Table 5.

3. Results and discussion

3.1. Effect of variation in the absorber, ETL, HTL and optimized absorber thickness

The SCAPS simulations were done on the basis of primary basic parameters as tabulated in Table 1, Table 2 and Table 3. The effect of thickness of absorber, ETL and HTL is very crucial in case of perovskite solar cell hetrostructures and reported in the literature with enhanced values of necessary parameters viz. %PCE, %FF, J_{sc} and V_{oc} [19–21]. In the case of variation in absorber thickness, we have taken all the basic parameters as per Table 1 and Table 3. The variation in the absorber thickness from 200 to 800 nm is shown in Fig. 3 for the required parameters i.e., %PCE, %FF, J_{sc} and V_{oc}.

It is depicted from Fig. 3(a–d) and supplementary material (TS1) that the Voc, Jsc and %PCE is increasing from 0.4530- 0.4714 V, 17.85–25.77 mA/cm^2 and 4.47%–6.12%, respectively with the increase in the thickness of absorber from 200-800 nm and the %FF values are showing decreasing (55.19%–50.38%) trend. This may be explained on the basis that more material is exposed in this case to light and therefore more energy will be absorbed in this layer. As a result of it, more electron-hole pairs will be generated with enhanced electron mobility [16,19,20]. The decrement in %FF is basically due to the internal recombination inside the lead-free perovskite material, generated due to the short life time of electron (t_n) and hole (t_p) charge carriers, which do not permit adequate period for charge carrier to develop conduction band at lead-free perovskite material.

The enhanced variation in %PCE with the thickness of absorber layer may be explained on the basis of significant decrease in %FF and increase in J_{sc} values. It is confirmed from this data that the 800 nm thicknesses of absorbing layer ($FASnI_3$) has better absorbing performance and higher PCE (6.12%) with FF (50.38%) and J_{sc} (25.77 mA/cm^2) parameters value.

Fig. 3(e–h) and supplementary material (TS2) depict the variation in the thickness of the ETL (TiO_2), which is much more crucial as per the reported experimental results very recently [16,19,20,36]. Herein the ETL variation, we have taken all basic parameters as in Table 1 and Table 3 including the optimized absorber thickness (800 nm). The variation in ETL thickness (10–40 nm) confirms the overall decrease in the performance parameters i.e., J_{sc}, V_{oc}, %FF and %PCE from 26-25.70 V, 0.6977–0.4405 mA/cm^2, 48.33%–48.24% and 8.64%–5.46%, respectively. There is only considerable slight variation observed in the J_{sc}, V_{oc} and %FF values. It is basically due to the uniform number of charge carriers produced in the lead-free perovskite material and

Table 5
Final device performance on the basis of optimized parameters.

Parameters	Present simulation	Absorber	ETL	HTL	Finally Optimized
J_{sc} (mA/ cm^2)	20.75	30.76	30.80	31.06	31.20
V_{oc} (V)	0.2745	0.7912	1.66	1.78	1.81
FF (%)	39.16	64.94	36.22	34.16	33.72
PCE (%)	2.23	15.81	18.57	18.97	19.08

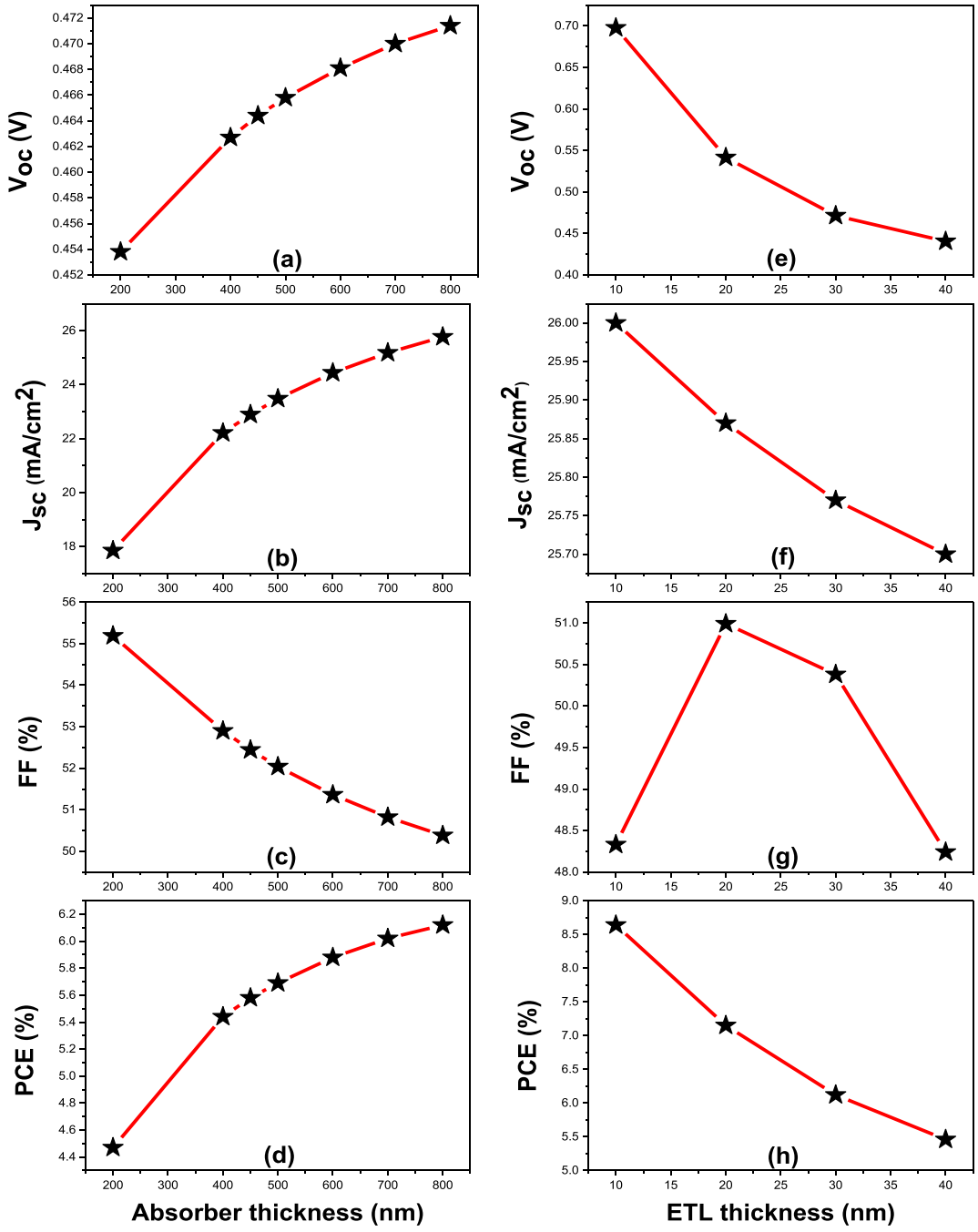

Fig. 3. (a-d) Variation in the absorber thickness with respect to performance parameters, keeping the fix ETL and HTL thickness, and **(e-h)** ETL thickness variation with respect to performance parameters at the optimized absorber thickness.

considerable decrease in the %PCE values may be due to the more charge recombination at the ETL/Absorber interface [19,20].

The variation in HTL thickness (50–400 nm) is tabulated in supplementary material (TS1) and not shown in the figure because there is not any considerable change found in any performance parameter (J_{sc}, %FF and %PCE) except V_{oc}, changes from 0.6908 to 0.6837 V. The maximum PCE is obtained 8.65% at 50 nm. It is mainly due to the uniform number of charge carriers produced in the lead-free perovskite material layers [19,20].

Now in continuation to optimize the performance parameters, again the perovskite layer is varied at optimized thickness of ETL (10 nm) and HTL (50 nm) and rest basic parameters taken from Table 1 and Table 3. Fig. 4(a–d) and supplementary material (TS2) represent the variation in the optimized absorber thickness (1200–2000 nm) with respect to performance parameters (V_{oc}, J_{sc}, %FF and %PCE) and observed the considerable increase in V_{oc} = 27.42–28.54 V, J_{sc} = 0.7045–0.7152 mA/cm^2 and %PCE = 9.03%–9.32% and slight decrease in %FF from 46.75% - 45.63%. It is basically due to the optimized ETL and HTL layers including more energy absorbed by the absorbing layer and more area or thickness (2000 nm) is to be exposed in this case to light.

So, the final optimized thickness of absorber layer, ETL and HTL are 2000 nm, 10 nm and 50 nm, respectively at which the power conversion efficiency has maximum value ~9.32%. In the next section, we will consider the basic parameters with these optimized parameters.

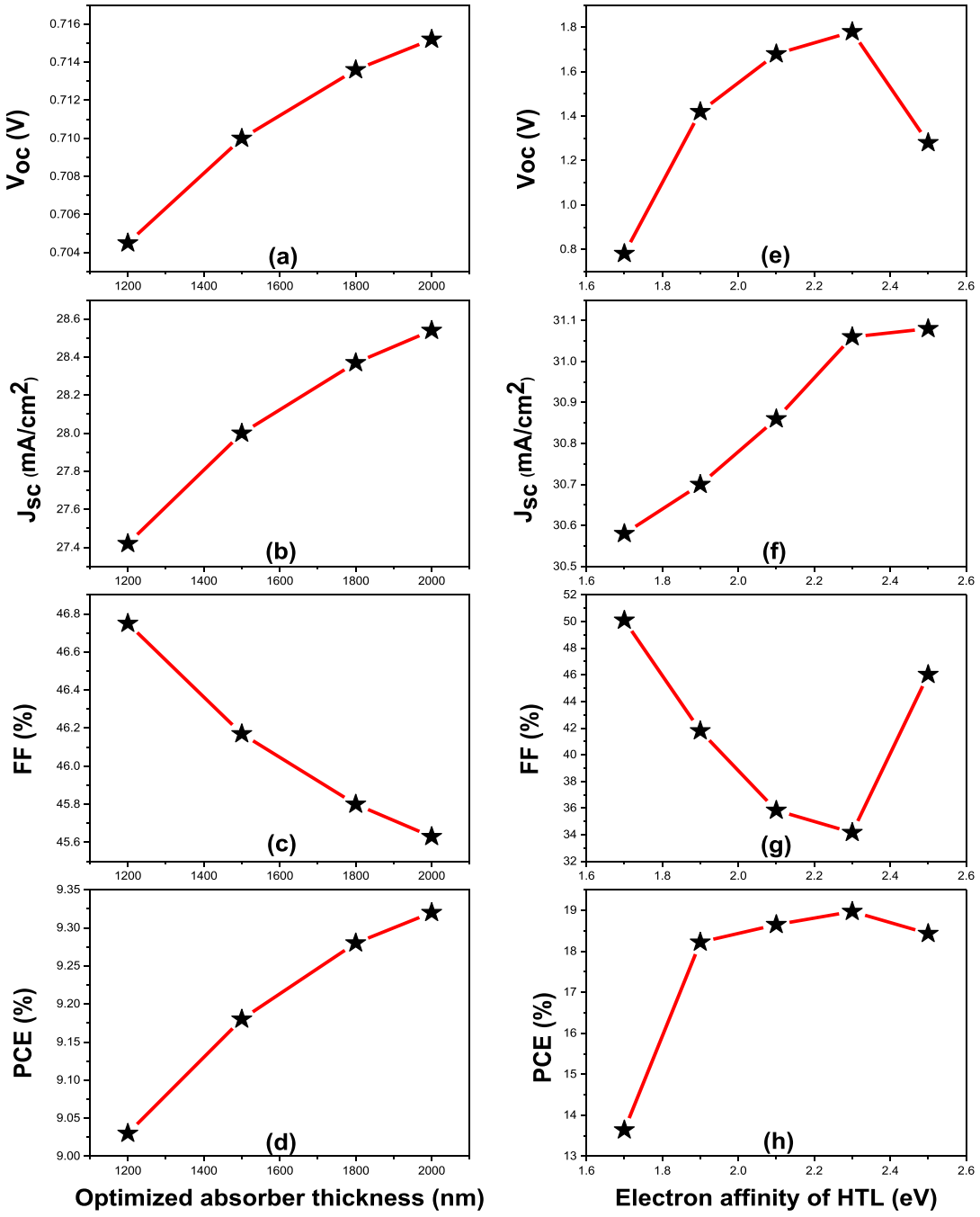

Fig. 4. (a-d) Variation in the absorber thickness at previously optimized absorber thickness (800 nm) including optimized ETL and HTL thickness, and **(e-h)** Variation in the affinity of HTL with respect to performance parameters at optimized thickness of absorber, ETL and HTL including defect density and doping (N_A) concentration of absorber.

3.2. Effect of variation in the concentration of defect density and doping (N_A) of absorber

As per the literature, the SRH (Shockley-Read-Hall) recombination has mainly governed the present absorber ($FASnI_3$) based devices. It is mainly cased of large defect density due to reduced film feature [37]. In such type of recombination, the carriers (holes and electrons) in valence and conduction bands, respectively recombined via trap states [38]. According to Zekary et al. [38], the longer diffusion length and less recombination are detected with decrease in defect density and increase in carriers life time (t_n and t_p). The conditions explained by Zekary et al. are the key factors to advance perovskite solar cell enactment [20,38]. Kang et al. have reported that the performance parameters can be optimized with a proper doping of metallic ions [39]. The variation in performance parameters is done with the help of SCAPS simulation and with the variation of the concentration of defect density (10^{14}-10^{16}) of absorber, tabulated in the supplementary material (TS3). Herein, the performance parameters J_{sc}, V_{oc} and %FF have the slight variation in the values but very necessary and crucial parameter %PCE has been optimized and have the value of 9.39% at 10^{15} defect density concentration in the absorber.

The doping is a very sensitive parameter for the influence on the

performance parameters. It can be increased, (never decreased)when reaction is in the process because decrease in the doping may not the practical process. In case of lead-free Sn-based perovskite, the oxidation of Sn^{2+} is observed in the air due to the high background carrier density [20]. With the increase of doping, there are two possible phenomena occurs at the interface and inside the layers [20], (i) more electrons and holes may take part in the reverse saturation current and enhanced its value and V_{oc} decreases, and (ii) the value of electric field at the hetrostructures interfaces increases and separation mechanism of carriers will be boosted. As a result of these mechanisms and increase in the recombination of the carriers, the reduced the performance of the device is seen. In the present case, variation in the doping (10^{14}-10^{16}) of absorber is observed and tabulated in the supplementary material (TS3). The optimum value of doping concentration is set 10^{15} and observed PCE = 10.90% is obtained.

3.3. Effect of variation in the affinity of ETL and HTL

The affinities of ETL and HTL have the great caliber to achieve good conversion efficiency as per the literature [19–22]. So, in the light it, we have done SCAPS simulation for the variation of affinity of ETL (3.5–3.9) and HTL (1.7–2.5). The values of V_{oc}, J_{sc}, %FF and %PCE are observed and tabulated in the supplementary material (TS4) including the plotted view for HTL variation in Fig. 4(e–h). It is seen from the supplementary material (TS1) for ETL that there is an optimized value of PCE = 18.57% at 3.7 affinity value. In case of HTL, highest value of conversion efficiency is achieved (18.97%) at 2.3 affinity value.

3.4. Other parameters

The capture cross section concentration of ETL/Absorber is already changed in the starting of simulation after the reported Table 2 parameters and change from 10^{-15} to 10^{-19} cm^{-2} for both carriers (electrons and holes) (Table 3) and achieved the enhancement in conversion efficiency from 2.23%-5.27%. So, in the light of it, we have now focused on the capture cross section concentration at interfaces of HTL/Absorber and $FASnI_3$ under optimized parameters. The capture cross section concentration of carriers at interfaces of HTL/Absorber changes from 10^{-15} to 10^{-19} cm^{-2} and for $FASnI_3$ from 2×10^{-14} to 2×10^{-19} cm^{-2}. After these changes in the capture cross section concentrations of electrons and holes at the interfaces, the optimized conversion efficiency is achieved a highest value (19.08%) and tabulated in Table 5.

3.5. Analysis of final optimized results

As a final point, the optimized basic parameters on the basis of sections 3.1-3.4 of this manuscript have been collected and repeated the SCAPS simulation for the optimum values for all performance parameters i.e., V_{oc}, J_{sc}, %FF and %PCE. The optimized performance parameters have been compared with the experimental [16] and theoretical [20] results and tabulated in Table 5. Fig. 5 shows the current-density vs voltage and quantum efficiency vs wavelength (inset) graphs of the finally optimized results and have the performance parameter values: V_{oc} = 1.81 V, J_{sc} = 31.20 mA/cm^2, %FF = 33.72 and %PCE = 19.08%. It is concluded from all the optimized results that the optimization of thickness of absorber, ETL and HTL and affinity of ETL and HTL play the crucial role in the performance enhancement of the cell.

4. Conclusion

In the present study, an organic-inorganic lead-free formamidinium Sn-based perovskite solar cell was systematically optimized and studied for better power conversion efficiency using SCAPS simulation. The effect of variation in thickness of absorber, ETL and HTL layer on the power conversion efficiency was studied and optimized thickness found to be ~2000 nm, 10 nm and 50 nm, respectively with a better power

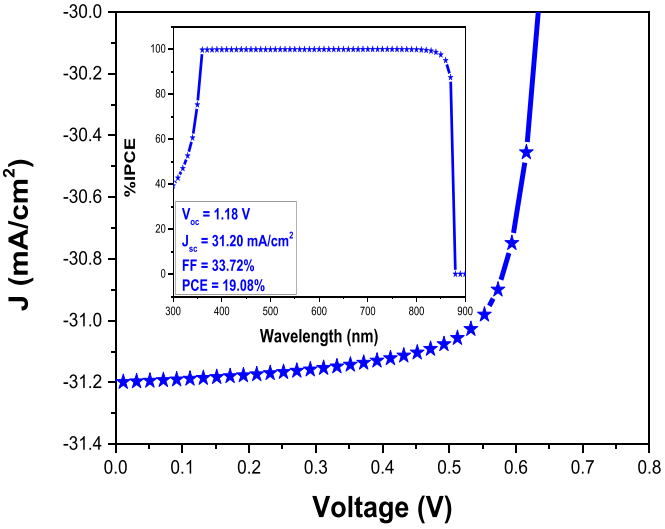

Fig. 5. Current density and quantum efficiency values of the finally optimized results.

conversion efficiency of ~9.32%. In continuation of optimizing the parameters to enhance the PCE, effect of variation in the concentration of defect density and doping (N_A) of absorber, affinity of ETL and HTL and capture cross section concentration were also studied and optimized. Overall, optimizing all these parameters in a very synchronous way, PCE value of ~19.08% was achieved along with enhanced short-circuit current density (J_{sc} = 31.20 mA/$cm^{2)}$, open-circuit voltage (V_{oc} = 1.81 V) and fill factor (%FF = 33.72%) which are essential component for realizing a good solar cell device. Results were also compared with the previous experimental and simulation data. Here, as compared to previous reported data, we have got enhanced value of PCE (~19.08%). Thus, the present study provides better results to be used to predict the lead-free perovskite solar cells-based devices in terms of better conversion efficiency value.

Ethics declarations

The manuscript is checked for plagiarism using licensed iThenticate software wide CSIR-NEERI Knowledge Resource Centre [KRC], Nagpur, India.

CRediT authorship contribution statement

Manish Kumar: Writing - original draft, Formal analysis. **Abhisek Raj:** Writing - original draft, Formal analysis. **Arvind Kumar:** Writing - review & editing, Formal analysis. **Avneesh Anshul:** Writing - review & editing, Formal analysis.

Declaration of competing interest

The authors declare that they have no known competing financial interests or personal relationships that could have appeared to influence the work reported in this paper.

Acknowledgments

The authors would like to thank Marc Burgelman, ELSI, University of Gent, Belgium for providing the SCAPS simulation software (Version: February 13, 2019). Author (M. Kumar) is thankful to University of Delhi, New Delhi for funding through Star Innovation Project (ARSD-SIP-01). One of the authors, A. Kumar also wants to acknowledge the financial support received from the UGC in form of UGC-BSR Research

Start-up Grant (F.30-374/2017(BSR)), New Delhi, India.

Appendix A. Supplementary data

Supplementary data to this article can be found online at https://doi.org/10.1016/j.optmat.2020.110213.

References

[1] W. Sun, Y. Li, S. Ye, H. Rao, W. Yan, H. Peng, Y. Li, Z. Liu, S. Wang, Z. Chen, L. Xiao, Z. Bian, C. Huang, High-performance inverted planar heterojunction perovskite solar cells based on a solution-processed CuOx hole transport layer, Nanoscale 8 (2016) 10806–10813, https://doi.org/10.1039/c6nr01927g.

[2] C. Momblona, L. Gil-Escrig, E. Bandiello, E.M. Hutter, M. Sessolo, K. Lederer, J. Blochwitz-Nimoth, H.J. Bolink, Efficient vacuum deposited p-i-n and n-i-p perovskite solar cells employing doped charge transport layers, Energy Environ. Sci. 9 (2016) 3456–3463, https://doi.org/10.1039/c6ee02100j.

[3] N.G. Park, Perovskite solar cells: an emerging photovoltaic technology, Mater. Today 18 (2015) 65–72, https://doi.org/10.1016/j.mattod.2014.07.007.

[4] K. Akhiro, T. Kenjiro, S. Yasuo, M. Tsutomu, Organometal halide perovskites as visible-light sensitizers for photovoltaic cells, J. Am. Chem. Soc. 131 (2009) 6050–6051, https://doi.org/10.1021/ja809598r.

[5] NREL. https://www.nrel.gov/pv/cell-efficiency.html, 2020. (Accessed 10 April 2020). https://www.nrel.gov/pv/cell-efficiency.html.

[6] P.K. Nayak, S. Mahesh, H.J. Snaith, D. Cahen, Photovoltaic solar cell technologies: analysing the state of the art, Nat. Rev. Mater. 4 (2019) 269–285, https://doi.org/10.1038/s41578-019-0097-0.

[7] D. Zhou, T. Zhou, Y. Tian, X. Zhu, Y. Tu, Perovskite-based solar cells: materials, methods, and future perspectives, J. Nanomater. 2018 (2018), https://doi.org/10.1155/2018/8148072.

[8] A. Babayigit, A. Ethirajan, M. Muller, B. Conings, Toxicity of organometal halide perovskite solar cells, Nat. Mater. 15 (2016) 247–251, https://doi.org/10.1038/nmat4572.

[9] Q. Zhang, F. Hao, J. Li, Y. Zhou, Y. Wei, H. Lin, Perovskite solar cells: must lead be replaced–and can it be done? Sci. Technol. Adv. Mater. 19 (2018) 425–442, https://doi.org/10.1080/14686996.2018.1460176.

[10] W. Ke, M.G. Kanatzidis, Prospects for low-toxicity lead-free perovskite solar cells, Nat. Commun. 10 (2019) 1–4, https://doi.org/10.1038/s41467-019-08918-3.

[11] M. Abuhelaiqa, S. Paek, Y. Lee, K.T. Cho, S. Heo, E. Oveisi, A.J. Huckaba, H. Kanda, H. Kim, Y. Zhang, R. Humphry-Baker, S. Kinge, A.M. Asiri, M.K. Nazeeruddin, Stable perovskite solar cells using tin acetylacetonate based electron transporting layers, Energy Environ. Sci. 12 (2019) 1910–1917, https://doi.org/10.1039/C9EE00453J.

[12] C. Liu, J. Tu, X. Hu, Z. Huang, X. Meng, J. Yang, X. Duan, L. Tan, Z. Li, Y. Chen, Enhanced hole transportation for inverted tin-based perovskite solar cells with high performance and stability, Adv. Funct. Mater. 29 (2019) 1808059, https://doi.org/10.1002/adfm.201808059.

[13] N.K. Noel, S.D. Stranks, A. Abate, C. Wehrenfennig, S. Guarnera, A.A. Haghighirad, A. Sadhanala, G.E. Eperon, S.K. Pathak, M.B. Johnston, A. Petrozza, L.M. Herz, H. J. Snaith, Lead-free organic-inorganic tin halide perovskites for photovoltaic applications, Energy Environ. Sci. 7 (2014) 3061–3068, https://doi.org/10.1039/c4ee01076k.

[14] F. Hao, C.C. Stoumpos, D.H. Cao, R.P.H. Chang, M.G. Kanatzidis, Lead-free solid-state organic-inorganic halide perovskite solar cells, Nat. Photon. 8 (2014) 489–494, https://doi.org/10.1038/nphoton.2014.82.

[15] M.H. Kumar, S. Dharani, W.L. Leong, P.P. Boix, R.R. Prabhakar, T. Baikie, C. Shi, H. Ding, R. Ramesh, M. Asta, M. Graetzel, S.G. Mhaisalkar, N. Mathews, Lead-free halide perovskite solar cells with high photocurrents realized through vacancy modulation, Adv. Mater. 26 (2014) 7122–7127, https://doi.org/10.1002/adma.201401991.

[16] T.M. Koh, T. Krishnamoorthy, N. Yantara, C. Shi, W.L. Leong, P.P. Boix, A. C. Grimsdale, S.G. Mhaisalkar, N. Mathews, Formamidinium tin-based perovskite with low Eg for photovoltaic applications, J. Mater. Chem. A. 3 (2015) 14996–15000, https://doi.org/10.1039/C5TA00190K.

[17] W. Ke, C.C. Stoumpos, I. Spanopoulos, M. Chen, M.R. Wasielewski, M. G. Kanatzidis, Diammonium cations in the $FASnI_3$ perovskite structure lead to lower dark currents and more efficient solar cells, ACS Energy Lett. 3 (2018) 1470–1476, https://doi.org/10.1021/acsenergylett.8b00687.

[18] M.E. Kayesh, T.H. Chowdhury, K. Matsuishi, R. Kaneko, S. Kazaoui, J.-J. Lee, T. Noda, A. Islam, Enhanced photovoltaic performance of $FASnI_3$ -based perovskite solar cells with hydrazinium chloride coadditive, ACS Energy Lett. 3 (2018) 1584–1589, https://doi.org/10.1021/acsenergylett.8b00645.

[19] A. Hima, N. Lakhdar, B. Benhaoua, A. Saadoune, I. Kemerchou, F. Rogti, An optimized perovskite solar cell designs for high conversion efficiency, Superlattice. Microst. 129 (2019) 240–246, https://doi.org/10.1016/j.spmi.2019.04.007.

[20] S. Abdelaziz, A. Zekry, A. Shaker, M. Abouelatta, Investigating the performance of formamidinium tin-based perovskite solar cell by SCAPS device simulation, Opt. Mater. (Amst). 101 (2020) 109738, https://doi.org/10.1016/j.optmat.2020.109738.

[21] S. Rai, B.K. Pandey, D.K. Dwivedi, Modeling of highly efficient and low cost $CH3NH3Pb(I_{1-x}Cl_x)_3$ based perovskite solar cell by numerical simulation, Opt. Mater. (Amst). 100 (2020) 109631, https://doi.org/10.1016/j.optmat.2019.109631.

[22] M. Burgelman, P. Nollet, S. Degrave, Modelling polycrystalline semiconductor solar cells, Thin Solid Films 361–362 (2000) 527–532, https://doi.org/10.1016/S0040-6090(99)00825-1.

[23] D. Hui-Jing, W. Wei-Chao, Z. Jian-Zhuo, Device simulation of lead-free $CH_3NH_3SnI_3$ perovskite solar cells with high efficiency, Chin. Phys. B 25 (10) (2016) 108802, https://doi.org/10.1088/1674-1056/25/10/108802.

[24] A. Niemegeers, M. Burgelman (Eds.), Numerical Modelling of AC-Characteristics of CdTe and CIS Solar Cells, Conference Record of the Twenty Fifth IEEE Photovoltaic Specialists Conference, 1996, pp. 13–17, https://doi.org/10.1109/PVSC.1996.564274.

[25] M.D. Stamate, On the dielectric properties of dc magnetron TiO2 thin films, Appl. Surf. Sci. 218 (1) (2003) 318–323, https://doi.org/10.1016/S0169-4332(03)00624-X.

[26] Evaluation of new materials for electron and hole transport layers in perovskite-based solar cells through SCAPS-1D simulations, in: S. Bansal, P. Aryal (Eds.), IEEE 43rd Photovoltaic Specialists Conference (PVSC) June, 2016, pp. 5–10, https://doi.org/10.1109/PVSC.2016.7749702.

[27] P. Calado, A.M. Telford, D. Bryant, X. Li, J. Nelson, B.C. O'Regan, et al., Evidence for ion migration in hybrid perovskite solar cells with minimal hysteresis, Nat. Commun. 7 (Dec 22 2016) 13831, https://doi.org/10.1038/ncomms13831.

[28] K. Ozawa, S. Yamamoto, R. Yukawa, R. Liu, M. Emori, K. Inoue, et al., What determines the lifetime of photoexcited carriers on TiO2 surfaces? J. Phys. Chem. C 120 (2016) 29283–29289, https://doi.org/10.1021/acs.jpcc.6b10136.

[29] S. van Reenen, M. Kemerink, H.J. Snaith, Modeling anomalous hysteresis in perovskite solar cells, J. Phys. Chem. Lett. 6 (Oct 1 2015) 3808–3814, https://doi.org/10.1021/acs.jpclett.5b01645.

[30] S. Ravishankar, O. Almora, C. Echeverria-Arrondo, E. Ghahremanirad, C. Aranda, A. Guerrero, et al., Surface polarization model for the dynamic hysteresis of perovskite solar cells, J. Phys. Chem. Lett. 8 (Mar 2) (2017) 915–921, https://doi.org/10.1021/acs.jpclett.7b00045.

[31] Q. Lin, A. Armin, R.C.R. Nagiri, P.L. Burn, P. Meredith, Electro-optics of perovskite solar cells, Nat. Photon. 9 (2014) 106–112, https://doi.org/10.1038/nphoton.2014.284.

[32] D. Poplavskyy, J. Nelson, Nondispersive hole transport in amorphous films of methoxy-spirofluorene-arylamine organic compound, Appl. Phys. 93 (1) (2003) 341–346, https://doi.org/10.1063/1.1525866.

[33] D. Liu, T.L. Kelly, Perovskite solar cells with a planar heterojunction structure prepared using room-temperature solution processing techniques, Nat. Photon. 8 (2013) 133, https://doi.org/10.1038/nphoton.2013.342.

[34] Z. Zhao, F. Gu, Y. Li, W. Sun, S. Ye, H. Rao, et al., Mixed-organic-cation tin iodide for lead-free perovskite solar cells with an efficiency of 8.12, Adv. Sci. 4 (11) (2017) 1700204, https://doi.org/10.1002/advs.201700204.

[35] C. Kim, T.D. Huan, S. Krishnan, R. Ramprasad, A hybrid organic-inorganic perovskite dataset, Sci. Data 4 (2017) 170057, https://doi.org/10.1038/sdata.2017.57.

[36] L.M. Herz, Charge-carrier mobilities in metal halide perovskites: fundamental mechanisms and limits, ACS Energy Lett. 2 (7) (2017) 1539–1548, https://doi.org/10.1021/acsenergylett.7b00276.

[37] T.S. Sherkar, C. Momblona, L. Gil-Escrig, J. Avila, M. Sessolo, H.J. Bolink, et al., Recombination in perovskite solar cells: significance of grain boundaries, interface traps, and defect ions, ACS Energy Lett. 2 (5) (2017) 1214–1222, https://doi.org/10.1021/acsenergylett.7b00236.

[38] A. Zekry, A. Shaker, M. Salem, Chapter 1 - solar cells and arrays: principles, analysis, and design, in: I. Yahyaoui (Ed.), Advances in Renewable Energies and Power Technologies, Elsevier, 2018, pp. 3–56.

[39] A.K. Kang, M.H. Zandi, N.E. Gorji, Simulation analysis of graphene contacted perovskite solar cells using SCAPS-1D, Opt. Quant. Electron. 51 (2019) 91, https://doi.org/10.1007/s11082-019-1802-3.